Chapter 2

A Standard Two-Stage On-board EV Charger with Minimum Switch Count

2.1 Introduction

A two-stage topology is an optimal choice for an on-board electric vehicle (EV) charger as discussed in the literature survey in chapter 1. Considering the number of power semiconductor devices and properties like galvanic isolation, a two-stage topology is an optimal choice for an on-board EV charger. A generalized block diagram of standard two-stage EV charger is shown in Fig. 2.1. The first stage of this two-stage EV charger consists of an AC-DC conversion unit, which includes an AC-DC rectifier and a DC-DC boost converter with power factor correction (PFC). The second stage shows a DC-DC conversion unit having galvanic isolation. This stage converts DC to high frequency AC and then back to DC. This allows a high frequency transformer to be included in the system for providing galvanic isolation.

The main features of a standard on-board EV charger is listed below:

i) PFC operation at the AC supply side.

ii) Galvanic isolation within the charger to restrict the supply side fault effects to reach up to the EV battery pack.

iii) Constant current – constant voltage (CC-CV) charging algorithm.

To accommodate these features, a novel two-stage standard on-board battery charger having minimum switch count, using a single controlled PWM signal is presented in this chapter for EV charging applications. The proposed charger draws power from a single-phase AC supply, which makes it more convenient for an EV user as single-phase AC supply is universally available [105].

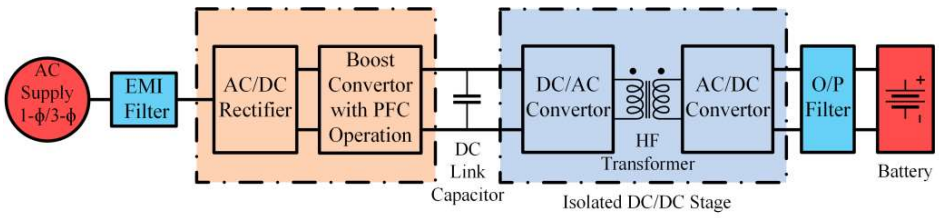

Fig. 2.1. Generalized block diagram of a two-stage standard EV charger.

The first stage of the prosed EV charger is responsible for AC to DC conversion with PFC operation, which consists of two switches and two diodes. The second stage is a DC-DC converter having a half-bridge LLC resonant configuration along with a high frequency isolation transformer. The proposed charger consists of only four switches and four diodes, which is minimum in terms of switch count among the reported chargers for EV applications. The conventional control strategy of EV charger requires multiple feedback loops for various stages. For example, a two-stage conventional EV charger requires at least two control loops for the complete operation of the EV charger. In order to simplify this complex control-loop issue, a novel control scheme named single controlled PWM technique (SCPT) is proposed in this chapter, which performs both the PFC operation as well as CC-CV optimal battery charging with a single controlled loop. Further, the conventional control techniques require multiple PWM signals for multiple power electronic switches. The proposed solution operates the entire charger, which manages both the PFC operation as well as CC-CV optimal battery charging with a single controlled PWM signal.

The details of the proposed EV charger including its mathematical modeling, analysis and operation are presented in this chapter. A 500 W scaled-down laboratory prototype is fabricated to validate the proposed concept. The proposed charger is tested to charge a battery set of 24 V, 30 Ah using CC-CV algorithm achieving a maximum efficiency of 97.6% in this chapter. The prototype is tested for resistive load at its rated power and the results for dynamically varying conditions are captured. A Texas Instrument TMS320F28335 DSP board is used for implementing the proposed control technique.

2.2 The Proposed Two-stage EV charger

The proposed two- stage EV charger topology is shown in Fig. 2.2. The role of the first stage is to convert the AC power drawn from grid to DC power with voltage boosting capability, while maintaining near unity power factor at the grid side. Existing literature suggest a diode bridge rectifier cascaded with a separate DC-DC boost converter for the purpose of AC-DC stage with PFC operation. However, in this work, a single stage AC-DC boost topology is used to serve the purpose of two separate sub stages using two switches, two diodes and a boost inductor at its input side. The main objective of the second stage in the proposed charger is to provide a constant gain with galvanic isolation in the DC-DC converter. For implementing SCPT, the second stage is required to be operated with a constant duty cycle. Among various resonant converters studied in [106]–[109] the LLC resonant converter is found to be the most

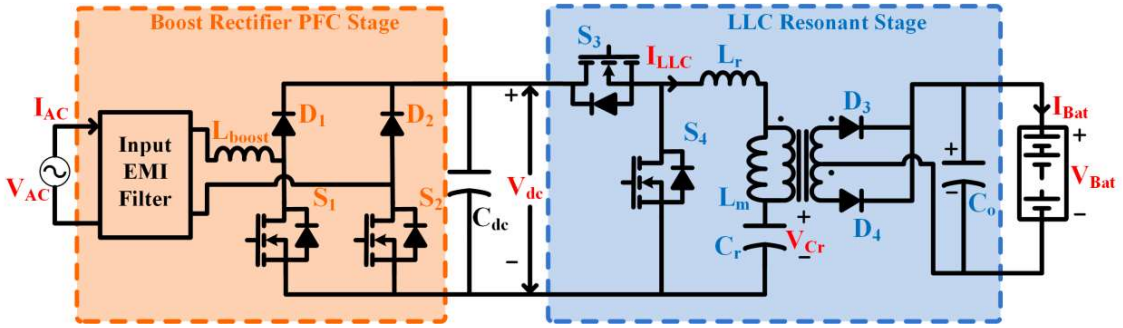

Fig. 2.2. Circuit Diagram of the proposed EV charger.

suitable candidate for this purpose. Providing the electrical isolation and having low switch count are the additional advantages of the half-bridge LLC resonant converter [110]. The second stage includes two switches and a center tapped transformer for the purpose of galvanic isolation. This stage also includes some passive elements to form a resonant network and two diodes at the secondary side for rectification purpose. Both the stages are cascaded by a DC-link capacitor. An EMI filter is used at the input side to avoid unnecessary electromagnetic interferences. A filter capacitor is used across the battery terminals for smoothing the output voltage.

The comparison of switching devices with existing literature is presented in Table 2.1. The combination of these two stages effectively reduces the number of switches and diodes in the proposed EV charger, which uses only four switches and four diodes, and is minimum among the existing topologies. All topologies presented in Table 2.1 have more number of switches and diodes as compared to the proposed charger, except the one presented in [45], which do not provide galvanic isolation between the input and output ports.

2.3 Operation and Analysis of the Proposed EV Charger

The operation of the complete topology can be explained in two phases for two power stages; (a) AC-DC boost converter and (b) half-bridge LLC resonant converter.

2.3.1 Operation of AC-DC Boost Converter

The operation of stage-I (AC-DC boost converter) is explained in four modes. The mode-1 and mode-2 correspond to the switch ON and switch OFF intervals during the positive half cycle of input AC supply voltage. Similarly, mode-3 and mode-4 correspond to the switch ON and switch OFF intervals during negative half cycle of input AC supply voltage.

Table 2.1 Switch Count Comparison with the available literature

Literature	Nature of AC Supply (1-ϕ or 3ϕ)	Number of Stages in the EV Charger	Galvanic Isolation	Number of Controlled Switches	Number of Uncontrolled Switches	Total Number of Switches
[26]	1-phase AC	1	Yes	6	16	22
[28]	3-phase AC	3	No	2	8	10
[44]	3-phase AC	3	No	16	0	16
[45]	1-phase AC	2	No	6	0	6
[46]	1-phase AC	2	Yes	5	9	14
[50]	1-phase AC	2	Yes	12	0	12
Proposed	**1-phase AC**	**2**	**Yes**	**4**	**4**	**8**

During the positive half cycle of the AC supply voltage, switch S_1, diode D_1 and the body diode of switch S_2 (D_{S2}) are forward biased. In mode 1, switch S_1 is turned ON so that the input current gets a closed path through the source, inductor, node *A*, switch S_1, body diode D_{S2} and node *B* to charge the boost inductor as shown in Fig. 3 (a). The diode D_1 is reverse biased during mode 1 as the DC-link voltage is applied across it in the reverse direction. At the same time, the DC-link capacitor supplies energy to the second stage. In mode 2, when the switch S_1 is turned OFF during positive half of AC supply, the AC source and the boost inductor supply energy to the second stage through D_1 and D_{S2} as shown in the Fig. 3 (b). This operation can also be understood by comparing it with the conventional DC-DC boost converter.

During the negative half cycle of the AC supply voltage, switch S_2, diode D_2 and the body diode of switch S_1 (D_{S1}) are forward biased. In mode 3, the S_2 is turned ON to charge the boost inductor through source, node B, S_2, D_{S1}, node A and inductor as shown in the Fig. 3 (c). Similarly, in mode 4, S_2 is turned OFF so that both the AC source and the boost inductor jointly supply energy to the second stage through the D_2 and D_{S1} as shown in the Fig. 3 (d).

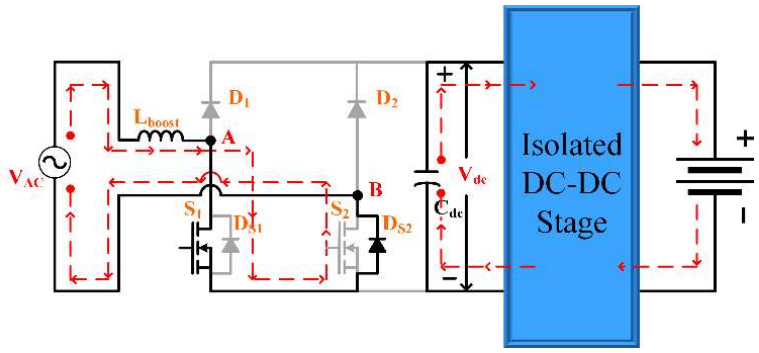

(a) Mode 1 (Positive half cycle; Switch S1 ON)

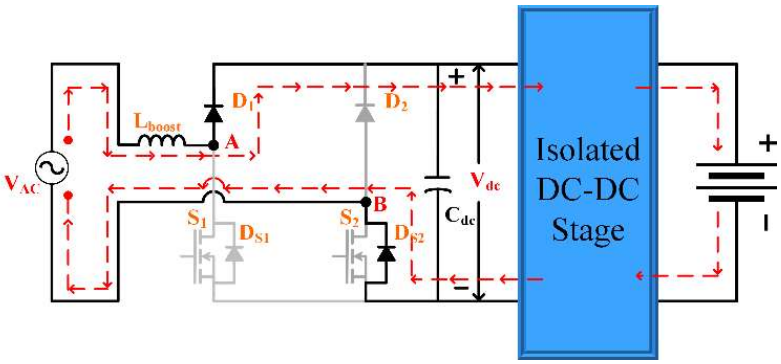

(b) Mode 2 (Positive half cycle; Switch S1 OFF)

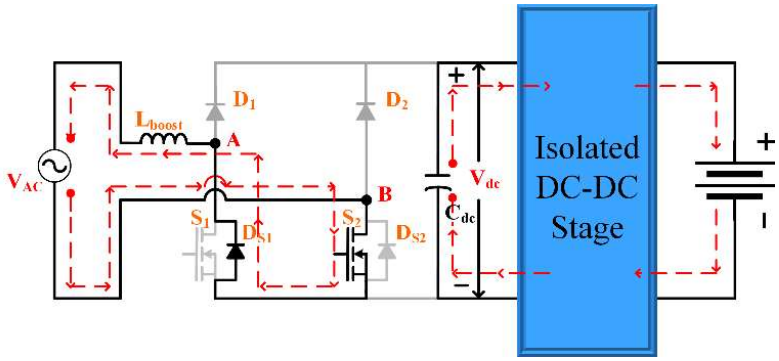

(c) Mode 3 (Negative half cycle; Switch S1 ON)

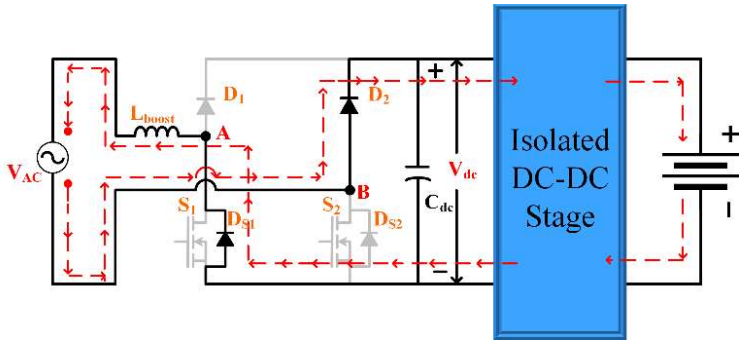

(d) Mode 4 (Negative half cycle; Switch S1 OFF)

Fig. 2.3. Modes of operation for AC-DC boost stage.

The voltage stress across the diodes D_1 and D_2 during mode-1 (S_1 ON) are same and equal to the DC-link voltage (V_{dc}). The current stress through the conducting devices (S_1 and D_{S2}) during this mode is the input current drawn from the source. Similarly, in mode-2, turning OFF of switch S_1 results into flow of current through the diode D_1 and the body diode of switch S_2 (D_{S2}) that flows through the load. During this mode, the voltage stress across the switch S_1 and the diode D_2 is V_{dc}. The ON and OFF operation of switch S_1 during the positive half cycle of input AC voltage can be compared with a traditional DC-DC boost converter and can be concluded that the voltage and current stresses across the switch is not high. In the similar way, the voltage and current stresses across different switches can also be estimated during the negative half cycle of input AC voltage.

2.3.2 Operation of Half-Bridge LLC Resonant Converter

In the proposed topology, a half-bridge LLC resonant converter is used as an isolated DC-DC converter for the second stage. This consists of a half-bridge switching network with resonant tank cascaded with an isolation transformer and a center-tapped diode rectifier as shown in the Fig. 2.4. The half-bridge switching network produces a square wave voltage that varies between zero and V_{dc}. This square wave voltage acts as the input to the LLC resonant circuit. The LLC circuit produces a sinusoidal current through it, when operated at its resonant frequency. The sinusoidal waves are then transferred to the secondary side of the isolation transformer and then center-tapped diode rectifier is used at the output side to charge the battery. Circuit diagram of the half-bridge LLC resonant converter with the load being transferred to the primary side is presented in Fig. 2.4.

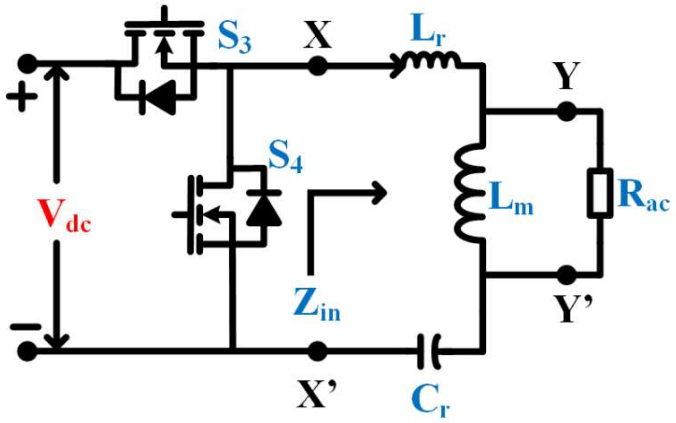

Fig. 2.4. Half-bridge LLC resonant Circuit.

Another advantage of using resonant converters is to ensure zero voltage switching (ZVS) operation to minimize the switching losses. To ensure ZVS, current through the switch must lag the voltage across it. So, from Fig. 2.4, the impedance seen by XX' must be inductive in nature [111]. The input impedance seen by XX' is given as,

$$Z_i = sL_r + (sL_m // R_{ac}) + \frac{1}{sC_r} \tag{2.1}$$

$$Z_i = \frac{s^3 L_m L_r C_r + s^2 (L_m + L_r) C_r R_{ac} + sL_m + R_{ac}}{s^2 L_m C_r + sC_r R_{ac}} \tag{2.2}$$

where

L_r is the resonant inductance used in series,

L_m is the mutual inductance in parallel with the load,

C_r is the resonant capacitor and

R_{ac} is the load resistance connected across YY'.

The Bode plot of Z_i is drawn at various load conditions to have a detailed idea on its operating frequency region and is shown in Fig. 2.5. The half-bridge LLC resonant circuit can have two resonant frequencies; f_{oc} and f_{sc}. From Fig. 2.5, it is clear that there are three operating regions of this converter: 1) frequency below f_{oc}; 2) frequency between f_{oc} and f_{sc}; and 3) frequency above f_{sc}.

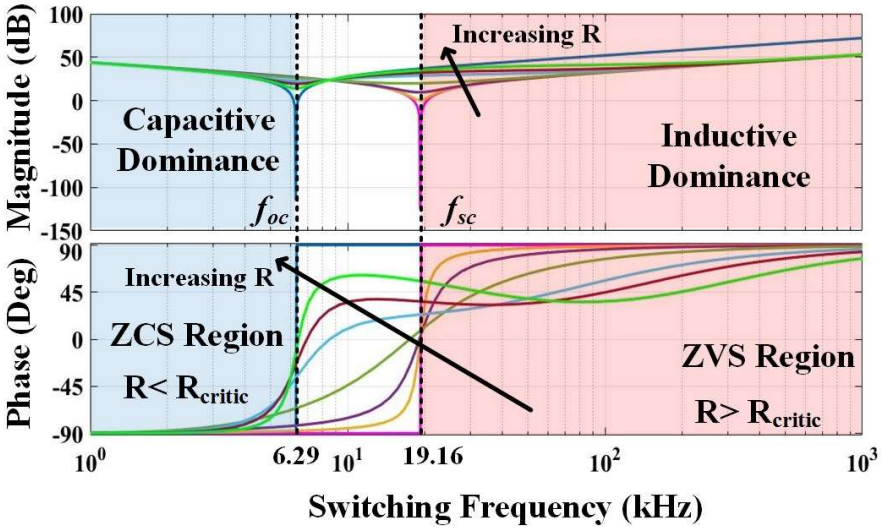

Fig. 2.5. Bode Plot of Zi.

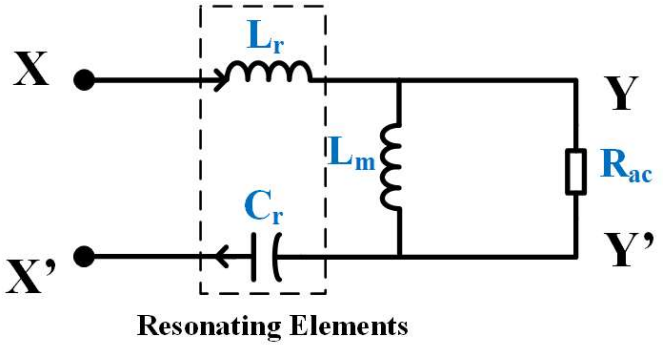

Fig. 2.6. The resonant circuit with load reflected from secondary side.

The concept of two resonant frequencies can be understood from the Fig. 2.6, where f_{oc} is the resonant frequency while R_{ac} is kept open. This indicates that R_{ac} is removed from the circuit and the transformer is not delivering power to the load. On the contrary, f_{sc} is the resonant frequency while R_{ac} is short circuited. This means L_m is cut-off from the circuit and power is transferred to the secondary side of the transformer. Hence, f_{oc} and f_{sc} can be expressed as follows:

$$f_{oc} = \frac{1}{2\pi\sqrt{(L_r+L_m)C_r}} \text{ and } f_{sc} = \frac{1}{2\pi\sqrt{L_r C_r}} \tag{2.3}$$

From the phase plot of Z_i, it is clear that the negative phase in the frequency range below f_{oc} shows the dominance of poles and hence Z_i shows a capacitive impedance. Similarly, positive phase in the frequency range above f_{sc} shows dominance of zeros, thus Z_i is inductive in nature. Therefore, to ensure ZVS operation, the half-bridge LLC resonant converter must be switched at a frequency more than or equal to f_{sc}. Thus, the operation of LLC resonant converter at its resonant frequency throughout the operating region facilitates smooth ZVS without using any voltage-controlled oscillator (VCO) or frequency modulation block.

2.4 Single Controlled PWM Technique (SCPT)

2.4.1 Background of SCPT

As discussed in earlier sections, a standard EV charger consists of two stages: AC to DC stage with built-in PFC operation and the DC-DC stage having isolation between the input and output ports. Both the stages are cascaded by a DC-link capacitor. For such standard EV chargers, two separate control loops are used for two different power stages as shown in Fig. 2.7, which requires multiple controlled signals for each stage. The first loop takes care of the intermediate DC-link voltage, while maintaining near unity power factor (UPF) operating condition. The second loop maintains constant voltage or constant current at the output port as

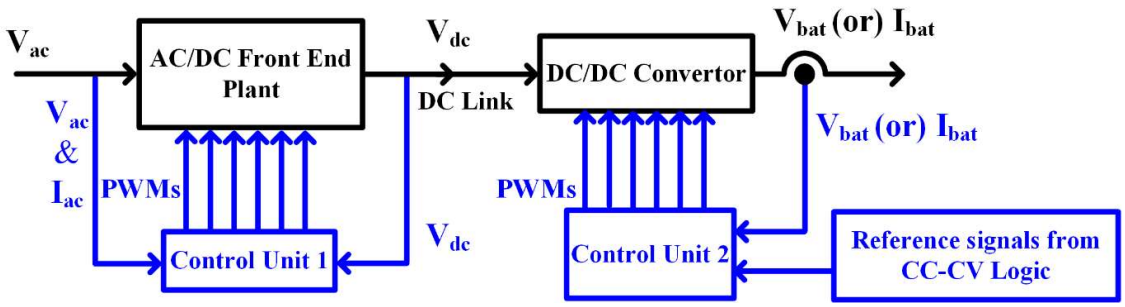

Fig. 2.7. Simplified block diagram of conventional control scheme.

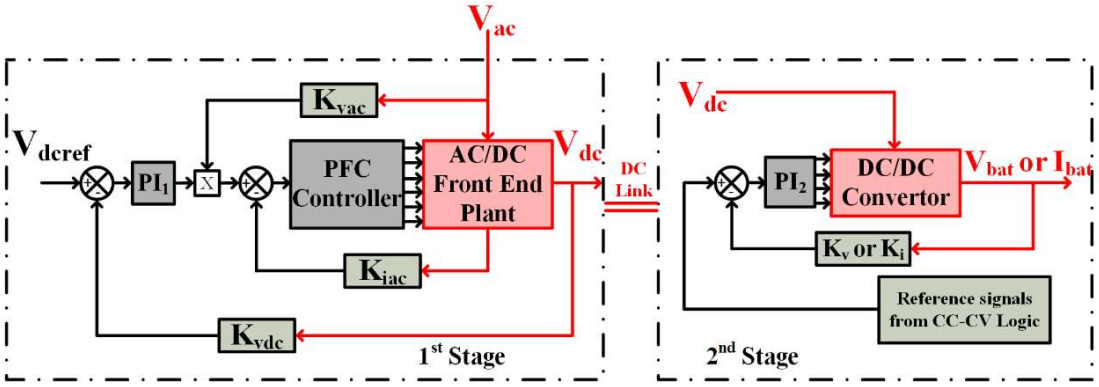

Fig. 2.8. Conventional control technique for EV Charger.

required by the CC-CV battery charging logic and is responsible for the switching from CC to CV mode, whenever required. The detailed operation of the conventional control scheme is elaborated in Fig. 2.8.

In Fig. 2.8, the intermediate DC-link voltage is sensed and fed to the proportional integral controller PI_1 that maintains the DC-link voltage (V_{dc}) according to its reference value (V_{dcref}). The input AC voltage serves as the reference signal for the input AC current and the PFC controller forces the input current to follow the input voltage wave shape to maintain near unity power factor at the input side. Similarly, the battery terminal voltage or battery terminal current is sensed and fed to the proportional integral controller PI_2, which is responsible for maintaining constant battery current during CC mode or constant battery voltage during CV mode. However, in case of the proposed SCPT, by considering the second stage as a constant gain converter, the intermediate DC-link voltage can be estimated from the battery voltage or the battery current sensed at the output port. Hence, the need of an additional sensor to sense the DC-link voltage can be eliminated and accordingly the need of an additional control loop is also avoided. The working principle of SCPT is demonstrated using a simplified block diagram as shown in Fig. 2.9.

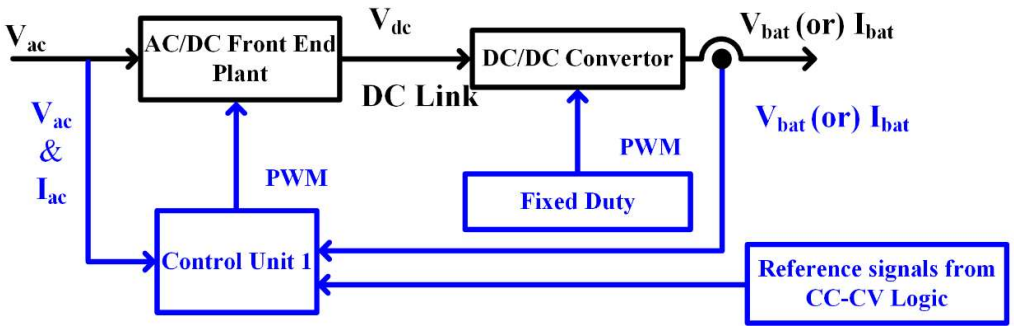

Fig. 2.9. Simplified block diagram of single controlled PWM technique.

Basically, a converter that operates with fixed duty cycle can be termed as a fixed gain converter or a constant gain converter. The resonant converters are found to be one of the most suitable candidates for obtaining constant gain, if they are operated at their respective resonant frequencies [112]. Most of the resonant converters provide galvanic isolation as demanded by a standard EV charger. Therefore, a suitable resonant converter is chosen for providing constant gain with galvanic isolation.

The advantages obtained by using the SCPT are: a) only one controlled PWM signal with single loop is used for the EV charger, b) mathematical complexities are reduced as the DC-DC stage operates at fixed duty cycle and hence the need of an additional controller is saved and c) need of the voltage sensor to sense the DC-link voltage is eliminated and thereby reduces the number of variables to be sensed.

2.4.2 Implementation of SCPT

To meet out the required constant gain of the half-bridge LLC resonant converter, it must be designed properly. Several methodologies are reported during the last decade to model the LLC resonant converters. However, this requires special design methods, as this converter operates based on the frequency modulation techniques, instead of pulse width modulation technique. Traditional methods like small signal analysis to model DC-DC converters are not helpful for resonant converters due to the above stated reasons. Various methods are reported in literature [113]–[115] to model the resonant converters. Most of these methods are either mathematically complex or an experimental prototype is needed before its design. Therefore, first harmonic approximation (FHA) is used to model the non-sinusoidal nonlinear circuit into a sinusoidal linear circuit [116], [117]. The only issue with this approximation is to run the circuit in the vicinity of short circuit frequency (f_{sc}) for satisfactory operation. As discussed

earlier, the resonant circuit needs to be operated on or above f_{sc} to ensure ZVS. Therefore, to implement SCPT with ZVS, the LLC resonant converter must be operated at f_{sc}.

The gain of the LLC resonant circuit can now be derived from the voltage division rule (as seen fromFig. 2.6) and is expressed as follows:

$$G_{LLC} = \frac{jX_{lm} \parallel R_{ac}}{(jX_{lm} \parallel R_{ac}) + j(X_{lr} - X_{cr})}$$

$$= \left| \frac{j\omega L_m \parallel R_{ac}}{(j\omega L_m \parallel R_{ac}) + j\omega L_r + {}^{1}/_{j\omega C_r}} \right| \tag{2.4}$$

The switching frequency (f_s) is normalized with respect to f_{sc} and is expressed as $f_n = {}^{f_s}/_{f_{sc}}$. The ratio of magnetizing inductance with the leakage inductance is considered as $L_n = {}^{L_m}/_{L_r}$ to easily formulate the expression of G_{LLC}. Now the expression for G_{LLC} can be rewritten as follows:

$$G_{LLC} = \left| \frac{L_n {f_n}^2}{\{(L_n + 1){f_n}^2 + 1\} + j\{({f_n}^2 - 1) f_n Q_c L_n\}} \right| \tag{2.5}$$

where Q is the quality factor of the circuit, which indicates the variation in load resistance (R_{ac}) and is defined as

$$Q = \frac{1}{R_{ac}} \sqrt{\frac{L_r}{C_r}} \tag{2.6}$$

In order to achieve a constant gain (G_{LLC}), the LLC resonant circuit is designed for the proposed charger by considering the minimum and maximum internal resistances of the battery, which is to be charged. Then, the gain of the LLC resonant circuit versus frequency plot is drawn. The same process is repeated for different loading conditions between the minimum and maximum values. These plots represent different loading conditions (different Q) across the LLC resonant circuit, which corresponds to different state of charge (SoC) during battery charging process. All these plots are presented in a single graph and are shown in Fig. 2.10. It is evident from Fig. 2.10 that all the curves merge to a single point at its resonating frequency and provides constant gain throughout the range of operation. Therefore, the LLC resonant converter is operated at its resonating frequency to achieve a fixed gain for different loading conditions throughout the charging process.

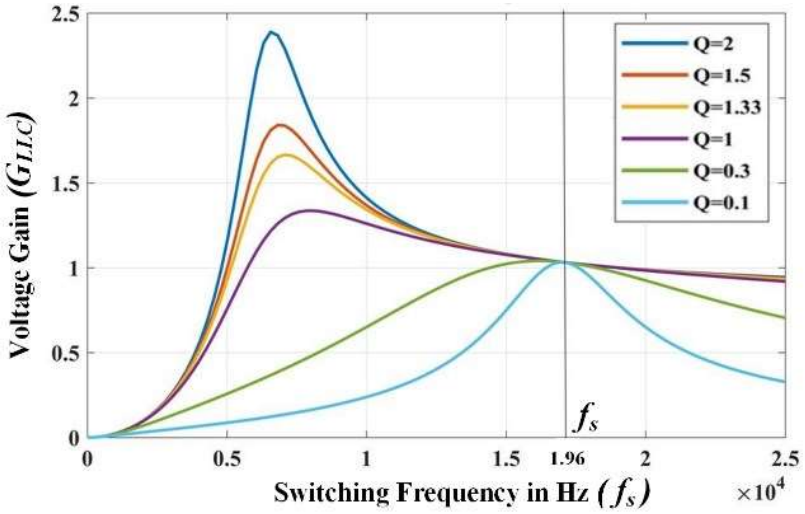

Fig. 2.10. Voltage gain of the LLC resonant converter for different Q-factor.

From the proposed schematic shown in Fig. 2.2, it is clear that the half-bridge configuration along with the isolation transformer having turns ratio (n) provides a gain of $0.5 \times n$ and the output diode rectifier with center tapped configuration provides a gain of 0.5. So, the overall gain of DC-DC converter is given as

$$G_s = 0.5 \times 0.5 \times n \times G_{LLC} \tag{2.7}$$

It is clearly observed from Fig. 2.10 that the gain of the LLC resonant network is unity, when operated at its short circuit resonance frequency (f_{sc}). Therefore, the gain of the second stage is given as

$$G_s = \frac{1}{4} n \tag{2.8}$$

From (2.8), it can be inferred that the gain of the second stage can be designed by selecting proper turn ratio of the transformer. The overall implementation of the SCPT for the proposed battery charger is shown in Fig. 2.11. The output terminal voltage or current is sensed from the battery end to regulate the intermediate DC-link voltage without sensing it. The gain of the LLC resonant converter G_s is divided with the sensed signal before comparing it with the reference signal generated from the CC-CV logic. The controller PI_1 is designed after deriving the open loop transfer function for the AC-DC boost converter as suggested in [118]. The output of the controller PI_1 is then multiplied with the AC voltage sensed from the input side and becomes the reference signal for the input current controller, which is responsible for near UPF operation of the charger. Because of this reason, the second controller is named as PFC controller.

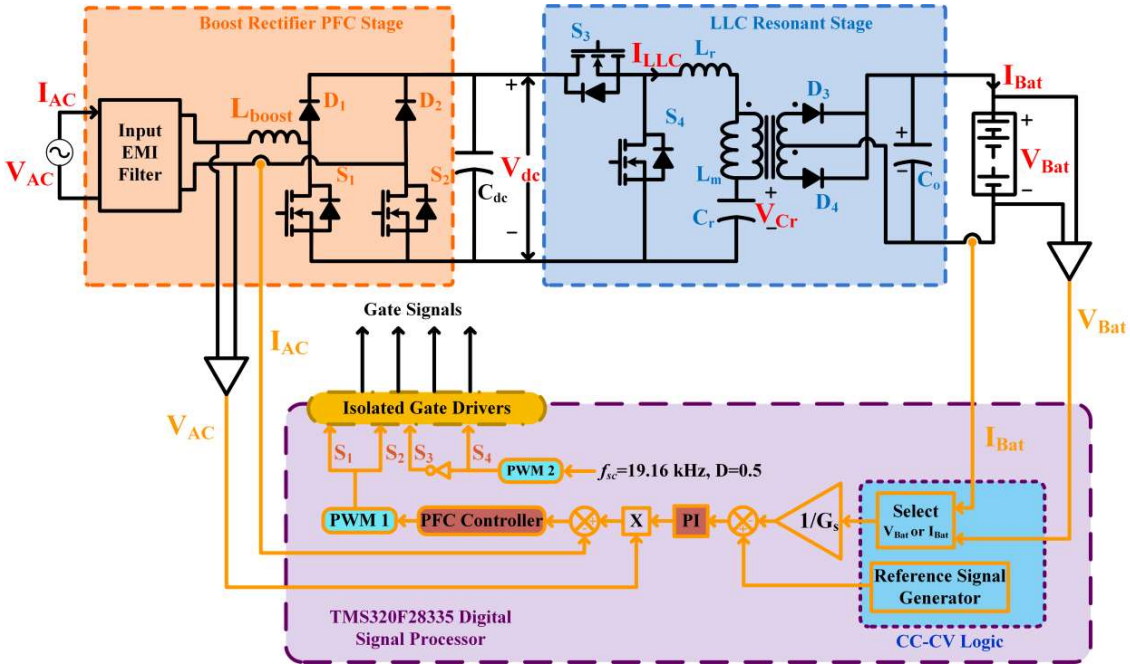

Fig. 2.11. Overall implementation of the proposed EV charger.

The switches S_1 and S_2 of the stage-I are operated alternatively during positive and negative half cycle. During the entire positive half cycle of AC supply, the voltage at source terminal of S_2 is at higher potential than the drain terminal, which is due to the nature of input voltage. In this case, D_{S2} conducts throughout the positive half cycle and S_1 turns ON and OFF according to the gate signal. Similarly, during the negative half cycle, D_{S1} conducts and S_2 turns ON and OFF according to the gate signal. In this way, simultaneous turn ON of S_1 and S_2 during a half cycle of operation is avoided in the AC/DC boost converter. Therefore, the same PWM signal is fed to S_1 and S_2 as shown in Fig. 2.11. Though the same PWM signal is fed to both the switches continuously, the switching operation is decided by the nature of input AC voltage whether it is in its positive or negative half cycle.

The half-bridge LLC resonant converter is operated with alternate 0.5 duty cycle having a dead time without requiring any control scheme. Hence, this stage just acts as a proportional block. With this, the need of an additional controller to operate the DC-DC stage is saved. This way of operating the second stage is one of the contributions of the proposed scheme and makes the second stage to work as a constant gain converter. Thus, the entire topology is operated with a single controlled PWM signal, which is fed to the switches S_1 and S_2.

2.5 Verification

The proposed charger is validated to charge a battery bank of 24 V. The bank consists of two 12 V, 30 Ah lead acid batteries. The overall implementation of the proposed charger is shown inFig. 2.11. A scaled down laboratory prototype is developed to demonstrate the proof of the concept. The component details used in developing the prototype is given in Table 2. 2. An E-core EE6527 with manganese-zinc ferrite material CF139 is selected for the transformer core and the turns ratio is kept at unity to achieve the desired output voltage. The number of turns used for both the primary and secondary sides are 10 for a maximum output voltage of 48 V. The core material performs optimally near 20 kHz, however based on the value of

Table 2. 2. Details of the components used

Components	**Rating**
DC-link Capacitor	1500 µF
Leakage Inductance (L_r)	69 µH
Mutual Inductance (L_m)	571 µH
Resonating Capacitor (C_r)	1 µF
Output Capacitor (C_o)	2000 µF
MOSFET (NTHL082N65S3F)	650 V / 40 A
Diode (40EPF06)	600 V / 40 A
Heat Sink	180 mm×123 mm×40 mm
Batteries	2 x (12 V, 30 Ah)
Gate Driver (FOD3182)	3 A
Voltage Sensors (AMC 1100)	320 mV
Current Sensors (ACS712ELCTR-05B-T, ACS713ELCTR-30A-T)	5 A, 30 A
Power Supply for Sensors, Gate drivers	5 V, 15 V
Voltage Regulator LM3940	5 V to 3.3 V

inductances of the transformer and available values of capacitor, the resonant frequency is fixed at 19.16 kHz, which is same as the switching frequency. A TI TMS320F28335 DSP is used to implement the proposed SCPT. The complete topology uses only one controlled signal fed to both the switches S_1 and S_2. The switches S_3 and S_4 are fed through a constant duty cycle of 0.5 at constant frequency and hence do not need any controller as shown in Fig. 2.11. The photograph of the laboratory developed prototype is shown in Fig. 2.12 and is tested at 470 W resistive load as well as for charging a 24 V, 30 Ah battery set.

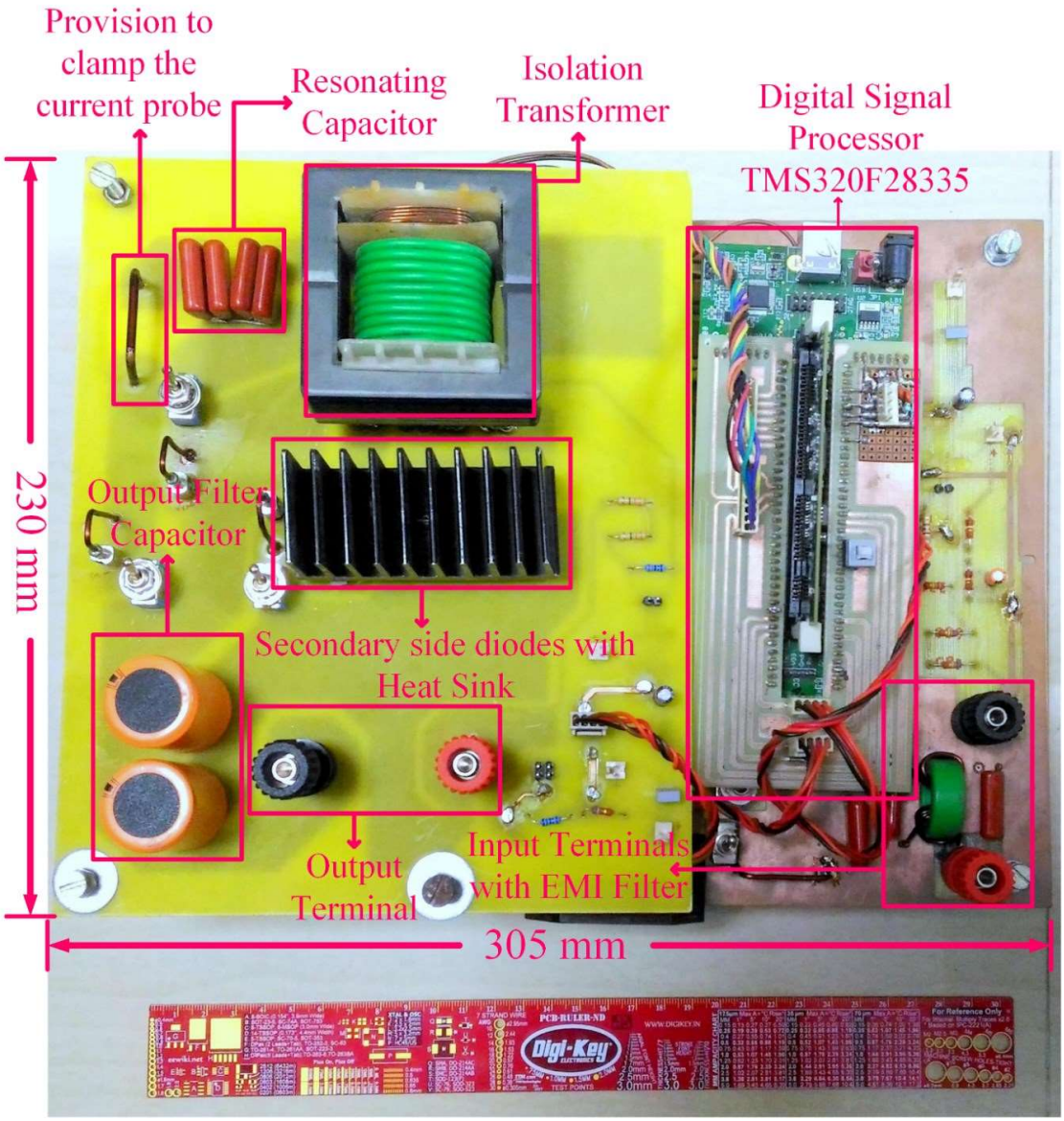

Fig. 2.12. Photograph of the lab developed prototype.

2.5.1 Proposed charger with resistive load

The prototype is tested with a resistive load of 5 Ω and an input AC voltage of 96.74 V (rms value). Fig. 2.13 shows the corresponding results. The input current drawn by the charger is 8.26 A (rms value) and is found to be in phase with the input voltage confirming the PFC operation. The DC-link voltage is measured to be 207.5 V, while the output voltage is 48.85 V.

The prototype is tested at 470 W with a resistive load and the result is shown in Fig. 2.14. The output voltage is found to be 48.0 V and the output current is found to be 9.71 A, when input rms voltage is 124.46 V and the rms current is 5.94 A. It is clearly observed from Fig. 2.13 and Fig. 2.14 that input current is sinusoidal and following the supply voltage, and thus maintains near UPF at its rated power.

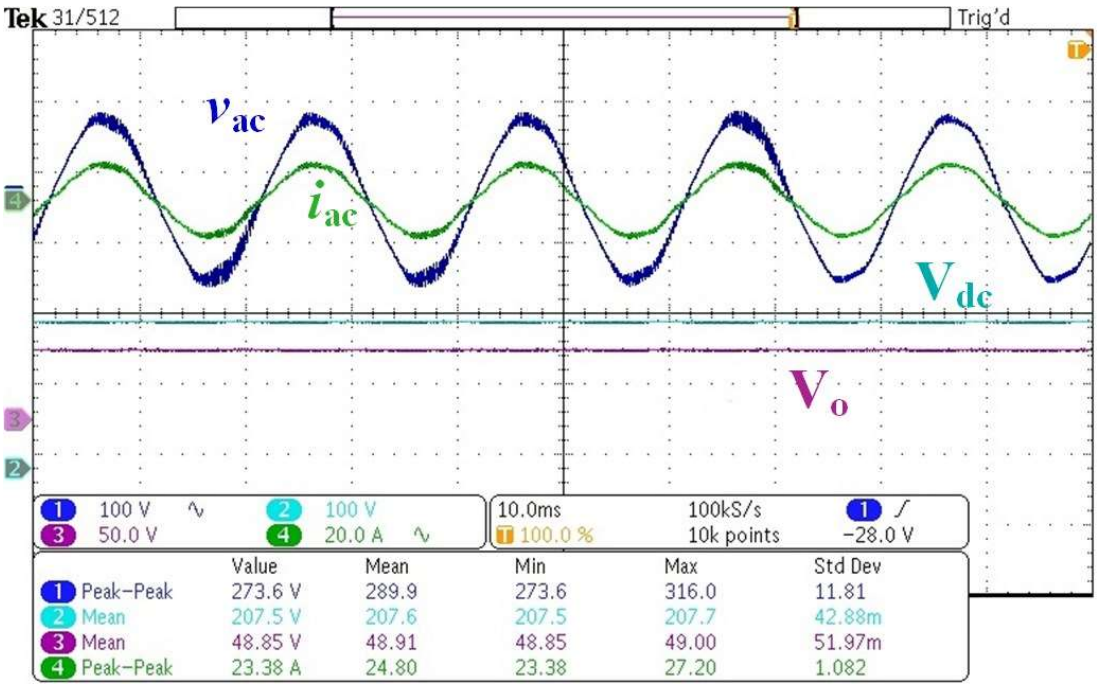

Fig. 2.13. Steady state waveform of Vdc= 207.5 V and Vo= 48.85 V with Input voltage Vac= 273.6 V (peak-peak), input current Iac= 23.38 A (peak-peak).

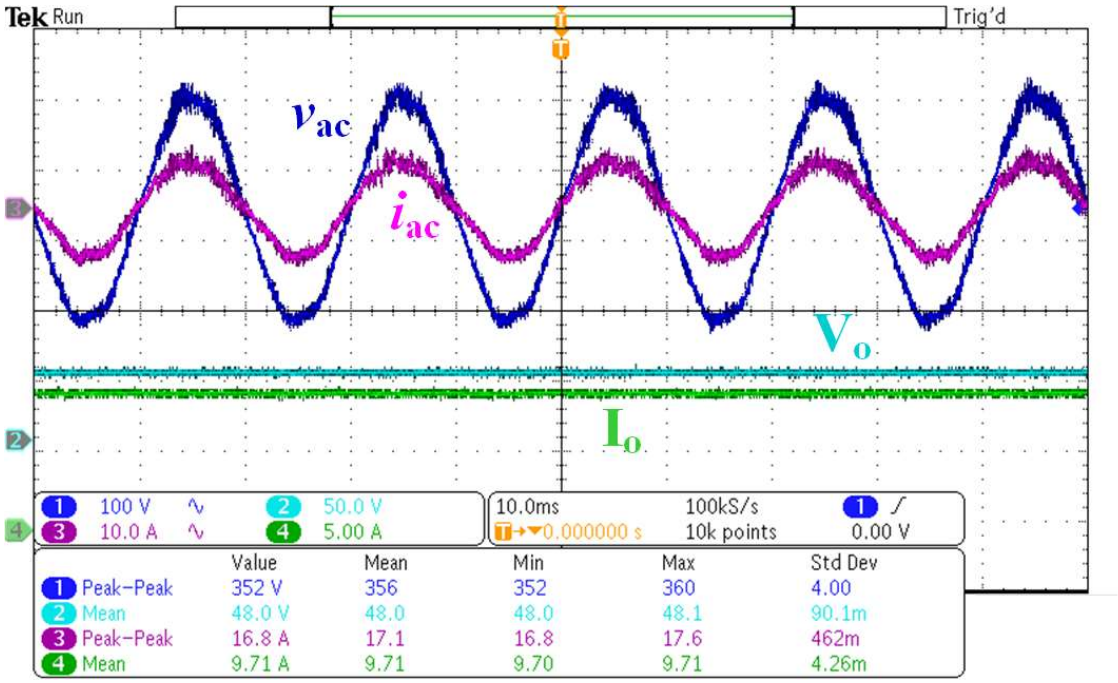

Fig. 2.14. Steady state output at 470 W resistive load. Output voltage Vo= 48 V, output current Io= 9.71 A, Input voltage Vac= 352 V (peak-peak), Iac= 16.8 A (peak-peak).

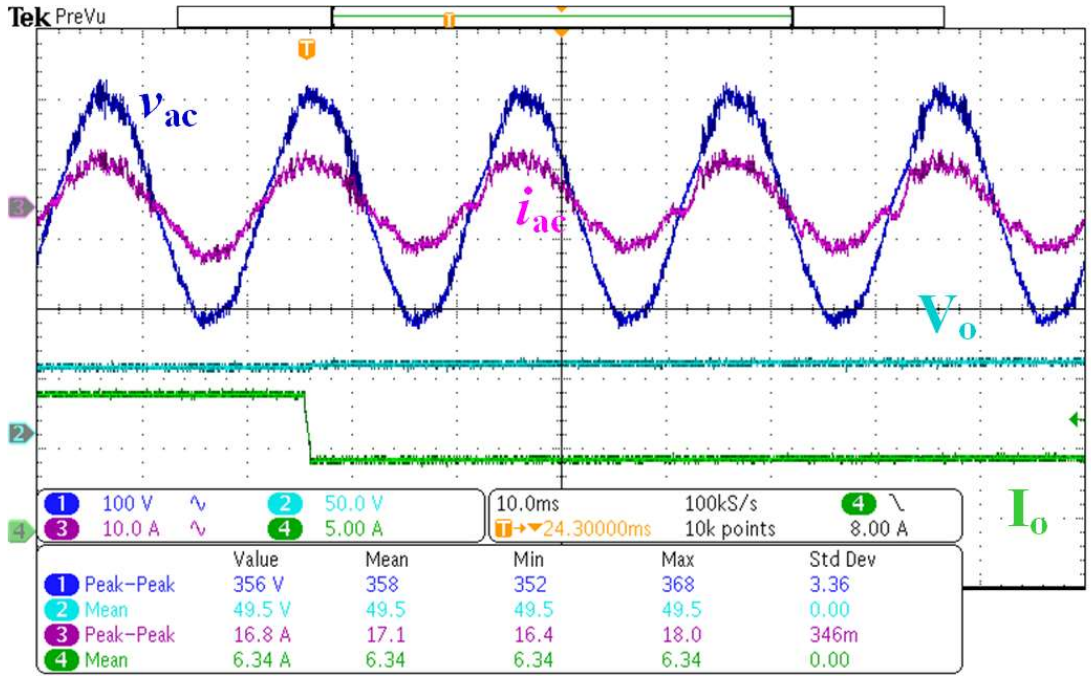

Fig. 2.15. Dynamics response while load current Io reduces by 50%.

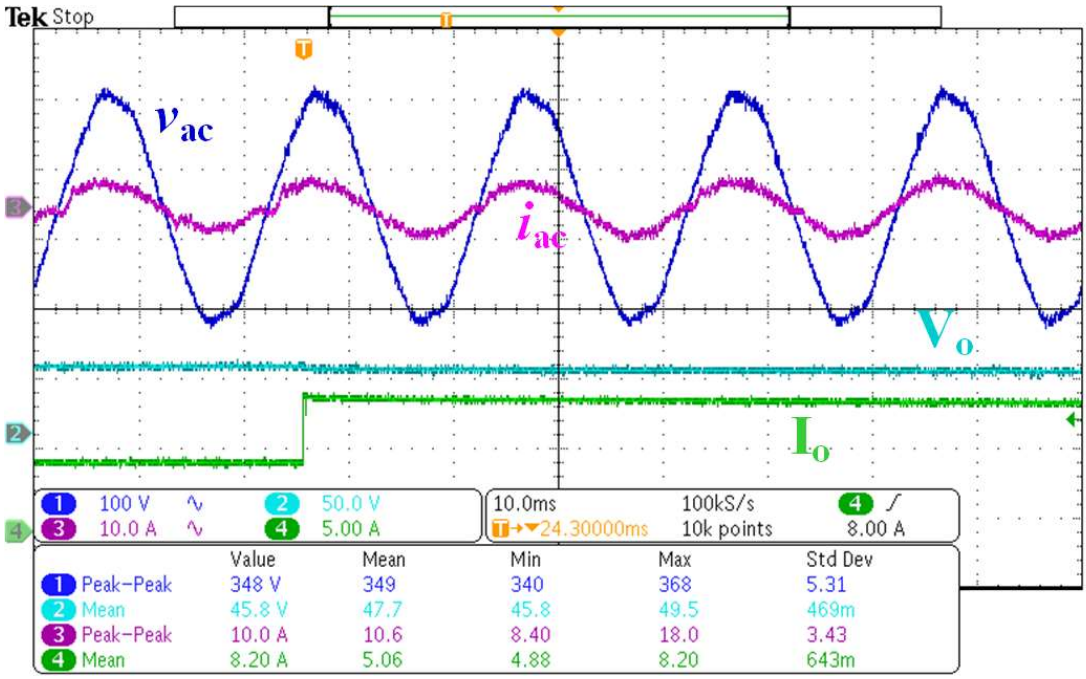

Fig. 2.16. Dynamics response while load current Io increased by 50%.

Fig. 2.15 and Fig. 2.16 show operation of the proposed EV charger under dynamic conditions. The EV charger is tested with 50% load change. The result shown in Fig. 2.15 is captured, when the load current decreases from 9.9 A to 4.95 A with output voltage of 49.5 V, while the input voltage and input current are 125.88 V (rms) and 5.94 A (rms) respectively. The sudden increase in load current from 4.58 A to 9.16 A is shown in Fig. 16 along with the input AC voltage of 123.05 V (rms) and input current of 3.53 A (rms). In both the cases, the PFC operations are satisfactory with stable output voltages and stable output currents.

2.5.2 Proposed charger for charging 24 V, 30 Ah lead acid battery

Fig. 2.17 shows the output and input voltages and currents during battery charging conditions. The battery current is regulated at 5.51 A, while the battery voltage is 27.5 V. Further, Fig. 2.17 confirms the PFC operation as the input current follows the supply voltage maintaining near UPF. The results for the second (DC-DC) stage of the EV charger are shown in Fig. 2.18.

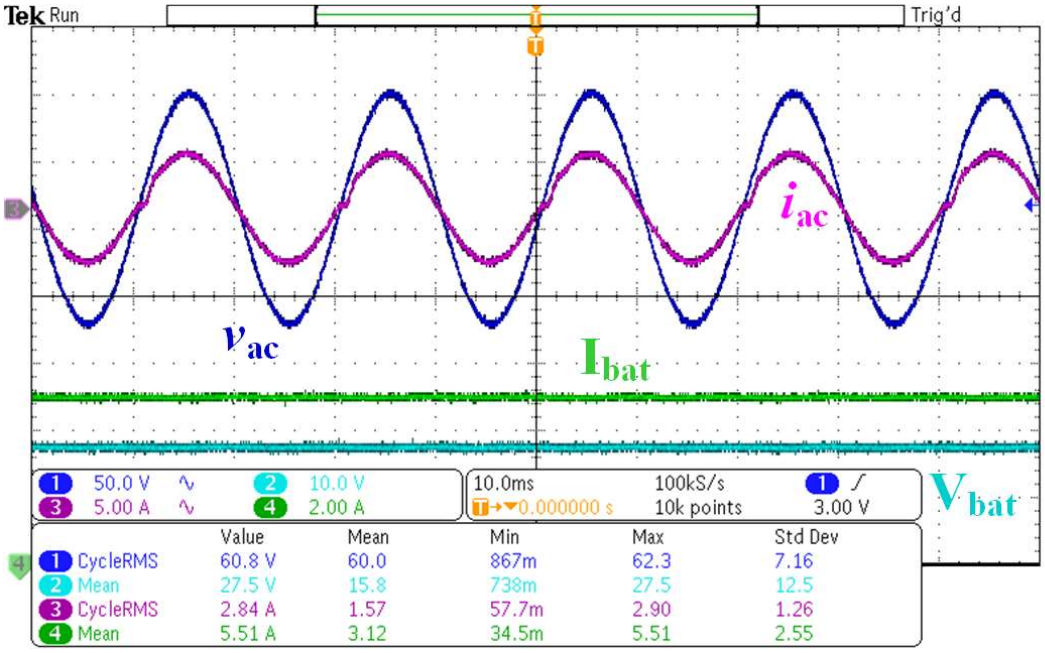

Fig. 2.17. Steady state waveform during battery charging. Input Voltage Vac= 60 V (RMS), input current Iac= 2.84 A (RMS), battery terminal voltage Vbat= 27.5 V, battery current Ibat=5.51 A.

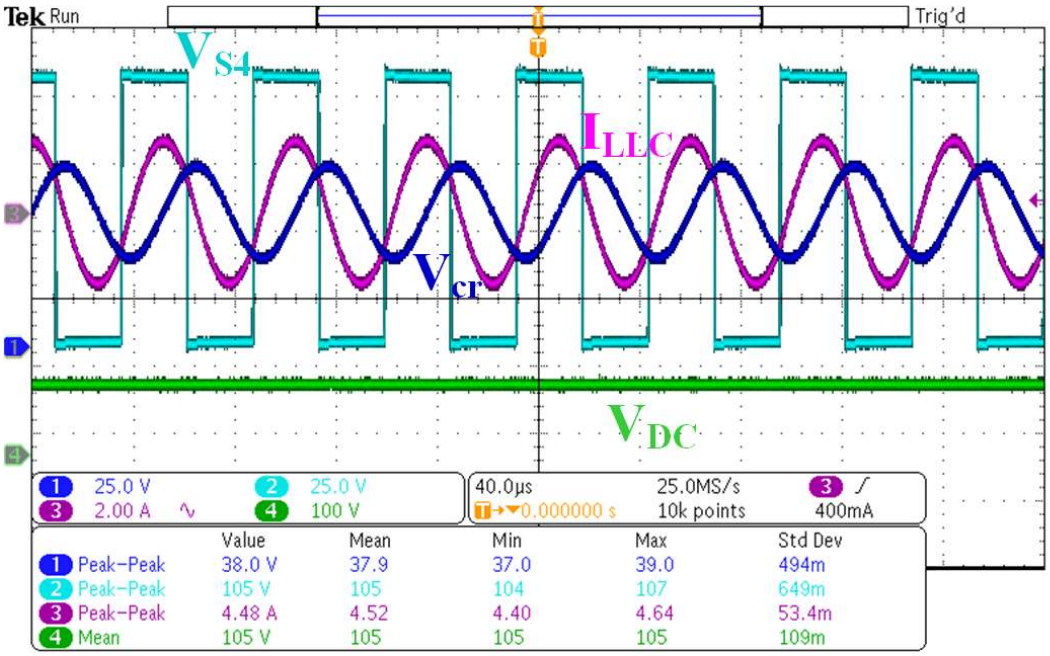

Fig. 2.18. Parameters of LLC resonance condition. DC-link voltage Vdc=105 V; Voltage across the switch S4 is a square wave of peak-peak =105 V. Voltage across Cr and current through LLC network show perfect sine waves.

Fig. 2.18 shows that the DC-link voltage is 105 V and the voltage across the switch S_4 is a square wave voltage varying between 0 V and 105 V. The current through the series resonant circuit (I_{LLC}) is sinusoidal and so is the voltage across the resonating capacitor (V_{cr}). In this way, the operation of resonant converter is confirmed.

The proposed EV charger behaves like a constant current source until the battery voltage reaches its full voltage (28.7 V). As soon as the battery voltage reaches 28.7 V, the entire topology behaves like a constant voltage source. The charger is operated in CC mode during low SoC of the battery and in CV mode during high SoC of the battery. Thus, the SCPT ensures constant voltage at the output terminal, while maintaining near UPF at the input. The SCPT also facilitates the smooth transition between CC and CV mode of charging. The CC-CV charging profile of the battery is shown in Fig. 2.19.

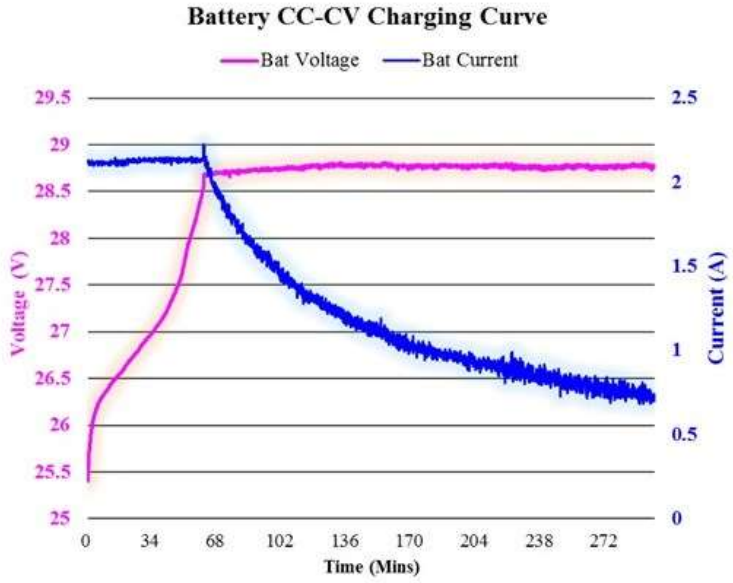

Fig. 2.19. Battery charging profile showcasing optimal charging using CC-CV logic.

The measurement of total harmonic distortion (THD) and the power factor (PF) are two important performance parameters of an EV charger. During the charging process, the values of THD and PF varies gradually according to the SoC of the battery [118], [119]. The value of THD lies at its minimum value at the beginning of charging and gradually increases with the increase in SoC. Similarly, the input PF decreases gradually with the increase in SoC. The THD of the input AC current for a charger should lie between 3% to 30% as suggested in [20], [119].

The THD at the beginning and at the end of the battery charging is measured using oscilloscope and presented in Fig. 2.20 and Fig. 2.21.

From the obtained results regarding THD and PF measurement, it can be inferred that the THD of input current drawn by the charger is found to be 3.38 % at the beginning and 14.1% at the end, which lies within the satisfactory limit of 3% to 30%. Similarly, at the beginning of measurement, the PF is found to be 0.991 and at the end of charging the PF is 0.975, which are found satisfactory.

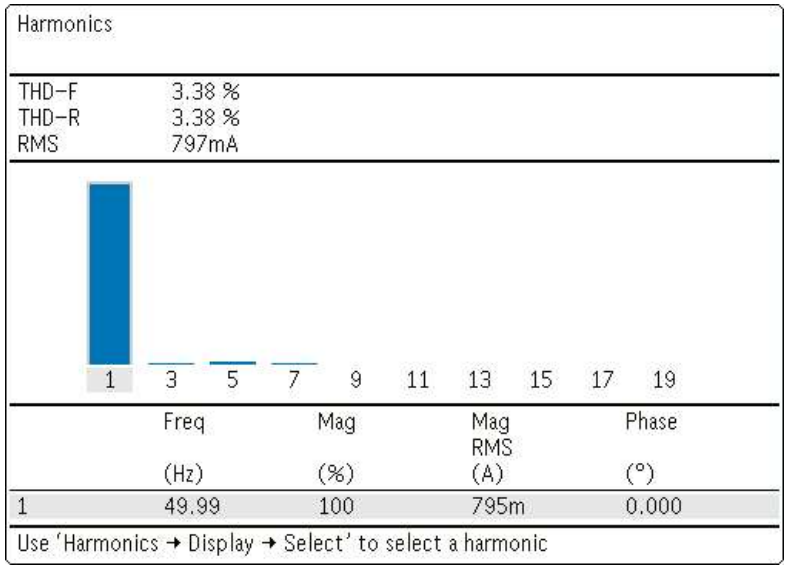

(a)

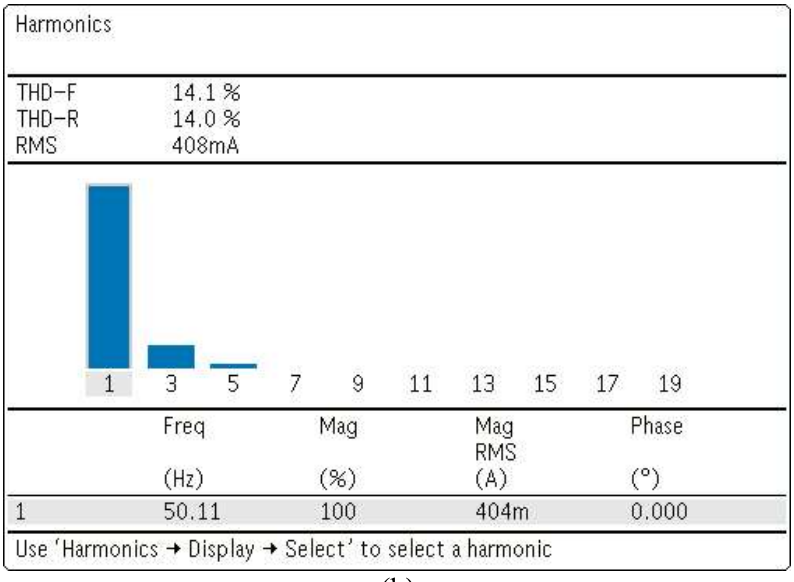

(b)

Fig. 2.20. THD measurement of the input current drawn from the grid.

Power Quality

	Value	Mean	Min	Max	Std Dev
V RMS	70.2 V	71.0	70.2	71.7	1.09
I RMS	801mA	801m	796m	828m	4.26m
Power Factor	991m	984m	976m	991m	10.7m

(a)

Power Quality

	Value	Mean	Min	Max	Std Dev
V RMS	71.8 V	73.4	71.8	76.9	1.08
I RMS	357mA	360m	356m	361m	1.43m
Power Factor	975m	972m	933m	977m	8.96m

(b)

Fig. 2.21. Measurement of PF at the input AC side.

2.5.3 Efficiency Analysis

The loss calculation across the power semiconductor devices for the proposed charger is carried out considering both the switching losses and conduction losses as suggested in [14]. During battery charging, the measured efficiency is found to be varying in nature over a range, as the SoC of the battery varies. Additionally, the efficiency also depends on the input AC voltage. So, a graph showing efficiency versus battery terminal voltage for different input voltage levels are shown in Fig. Fig. 2.22. It can be seen that Fig. 2.22 shows higher efficiency at higher AC input voltage level throughout the range of battery terminal voltage. A maximum efficiency of 97.6% is achieved, when the input voltage is 70 V and the battery terminal voltage is 28.7 V. It is also evident from the Fig. 2.22 that the efficiency increases as the SoC increases except at the last point, which is measured during the CV mode, as the battery is charged with trickle charging that draws less power as compared to the designed rating. The last point of each curves shows a dip because in any power electronic converter, the efficiency decreases, when operated at very low power as compared to the rated power.

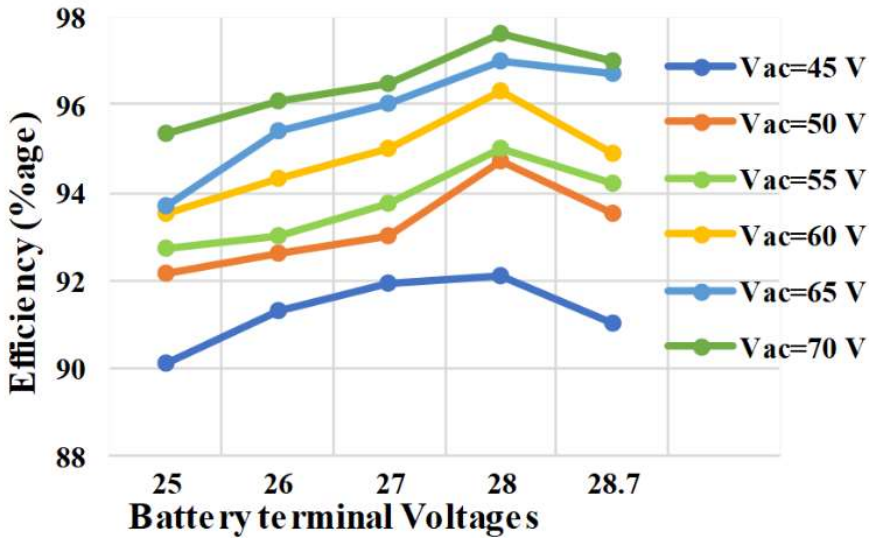

Fig. 2.22. Efficiency curves during battery charging at various input voltages.

2.6 Conclusion

A two-stage EV charger having minimum switch count using SCPT is presented in this chapter. First stage of the proposed charger is responsible for the AC-DC boost operation, while assuring PFC operation. The second stage of the charger provides galvanic isolation and maintains constant current or constant voltage at the battery terminal according to the CC-CV optimal battery charging logic. The SCPT reduces the mathematical complexities, as the DC-DC stage requires no controllers, unlike the conventional two-loop control strategy with multiple controlled PWM signals. Both PFC operation and optimal CC-CV charging are ensured using only a single controlled PWM signal. The detailed analysis of the proposed circuit is provided and its mathematical modelling is summarized in this chapter. A comprehensive comparison of the proposed charger with the existing chargers with similar topologies and the control techniques is provided in this study. The switch count in the proposed EV charger is found to be minimum as compared to the existing chargers. A scaled-down laboratory prototype is developed to validate the proposed work and its experimental results are included in this chapter. A maximum efficiency of 97.6% is achieved with this prototype for a 24 V, 30 Ah battery set.

Though, a two-stage on-board charger with minimum number of components is developed in this chapter, a propulsion module is essential to be on-board with the vehicle to drive the propulsion motor. Thus, in an EV with on-board charging feature, there are essentially

two power processing units are present in an EV. In order to replace two separate power-processing units for two operations, a single reconfigurable on-board power converter is presented in the next chapter for both the modes of operations.